

Identification of Particle Stimulated Nucleation during Recrystallization of AA 7050

D.P. Field¹, L. Behrens² and J.M. Root¹

Abstract: Mechanical properties of polycrystalline metals are dependent upon the arrangement of microstructural features in the metal. Recrystallization is an important phenomenon that often occurs during thermo-mechanical processing of metals. This work focuses upon aluminum alloy 7050 and uses crystallographic texture and pair correlation functions of recrystallized grains to characterize the dominance of particle stimulated nucleation in the recrystallization process. The randomization of the recrystallization texture and similar pair correlation functions for the particle distribution and the recrystallization nuclei distribution indicate that particle stimulated nucleation controls the recrystallization behavior in this alloy.

Keywords: AA 7050, recrystallization, electron backscatter diffraction.

1 Introduction

Optimization of microstructures through thermo-mechanical processing requires knowledge of the local stress-strain rate constitutive behavior of the material and how microstructures evolve under the given local deformation conditions. A basic feature of thermo-mechanically processed metals is that recrystallization can occur during processing, either dynamically or during inter-pass anneals. Recrystallization is an important phenomenon in commercial alloy systems because the mechanical properties of a product are often dependent on the fraction of recrystallized grains in the microstructure. Thick plates (>100 mm) of aluminum alloy 7050 and related alloys are commonly used in aerospace applications (eg. as wing spars) as this class of light weight alloys, when processed adequately, offers high strength and durability over a wide range of conditions. Several researchers have investigated structural evolution of AA 7050 during processing and much is known about this complex alloy [cf. Chakrabarti, et al, 1996, Gore, et al, 2003, Robson and Prangnell, 2001, Robson, 2004, and Beaudoin and Cassada, 1998]. The addition

¹ Washington State Univ, Pullman, WA, U.S.A.

² Purdue Univ, West Lafayette, IN, U.S.A.

of Zr to 7050 greatly retards the recrystallization process as the solute atoms and Zr rich dispersoids (typically fully coherent Al_3Zr) are effective at pinning grain boundaries, thereby inhibiting the formation and growth of new grains [eg. Riddle and Sanders, 2000].

Recrystallization nuclei form at positions of high orientation gradient and high stored energy in a metal. Relatively hard particles in the matrix that are of sufficient size to interrupt metal flow can lead to locally high orientation gradients and regions of high strain energy. This leads to particle stimulated nucleation (PSN) whereby recrystallization nuclei form preferentially at positions adjacent to particles in the structure [Humphreys, 1977, 1979, Ardakani and Humphreys, 1994]. The resulting microstructures consist of a somewhat randomized texture [Ørsund and Nes, 1988, Oscarsson, 1991] (or at least altered, if not predictable, texture [Engler, et al. 1997, Schafer, et al. 2009]) and often a smaller grain size since there is an increased density of nucleation sites for recrystallization. An understanding of when PSN mechanisms control the recrystallization process is important in accurate prediction of microstructural evolution.

Correlation functions provide a mathematical description of the spatial distribution of microstructural features. N-point correlation functions of structural features have been used by many researchers to accurately characterize mechanical, electrical and optical properties of various materials and to obtain bounds on effective properties [Beran, 1968, McCoy, 1981, Milton, 1981, Beran, et al. 1996]. Adams and co-workers have built on this early work and have led the push for including these measures in structural descriptions of polycrystalline materials [Fromm, et al. 2009, Adams, et al. 2008, Lemon, et al. 2007]. These measures are often a key component of microstructure-sensitive design using polycrystals that has been largely developed and championed by Adams and his colleagues.

The goal of the present effort is to quantify recrystallization kinetics and track the extent of PSN as a recrystallization nucleation mechanism in AA 7050. Texture and pair correlation functions are used to aid in the determination of the predominance of PSN in these structures. Texture considerations alone cannot generally be used to determine the extent of PSN in affecting the recrystallization behavior in relation to other nucleation mechanisms. It is anticipated that the addition of pair correlation functions in this analysis will assist in a more reliable quantification of this effect. The eventual goal of the work is to develop a model that tracks recrystallization of AA 7050 as a function of processing conditions to be able to process this alloy more efficiently and with the optimum microstructure for specific applications.

2 Experimental Details

Strips of metal were cut from the mid-thickness ($t/2$) and mid-width ($w/2$) section of hot rolled 127 mm (5 inch) thick plate of aluminum alloy 7050. The metal had been rolled from an ingot of initially 508 mm thickness (20 inches) using standard industrial rolling conditions. The nominal composition of the alloy was 5.7% Zn, 2% Cu, 1.9% Mg, 1.2% Zr and trace amounts of Si, Fe, Mn, Cr, and Ti with the remainder being aluminum. The metal strips were 10 mm in height with a width of 15 mm and a length of approximately 127 mm. The specimens were machined such that their heights and lengths aligned with the original normal and rolling directions of the plate. The specimens were then cold rolled an additional 10% to a final height of 114.3 mm.

After being cold rolled, the specimens were cut into smaller pieces using a slow speed diamond saw to obtain specimens of about 1 mm thickness. These specimens were rapidly heated in annealing salts at temperatures of 350°C, 450°C, and 500°C and held at temperature for various time durations ranging from 30 seconds to 24 hours (86,400 seconds). Immediately after annealing for given lengths of time, the specimens were quenched in water. The thin aluminum specimens make it reasonable to assume that both heating and quenching occurred in a nearly instantaneous manner, so recovery during heating to the recrystallization temperature did not occur.

Specimens were etched using Keller's etch to obtain optical images. Specimens were then re-polished to remove the effects of etching and to allow for measurements by automated electron backscatter diffraction (EBSD) analysis. EBSD was performed using a thermal source, field emission scanning electron microscope with scans being taken over a regular hexagonal array of measurement positions with a spacing of 2 – 10 μm . Analysis areas for each scan were on the order of 10^5 – 10^6 μm^2 .

3 Results and Discussion

By examination of the optical images and utilizing a line-intercept approach, the recrystallization fraction was measured for each annealing time and temperature. The recrystallization rate was slow for all temperatures, so data shown in the present study are only those from the highest annealing temperature (500°C) with the most rapid recrystallization kinetics. Fig. 1 shows a chart containing all of the raw data obtained for the material recrystallized at 500°C as well as a trend line fit to a standard Avrami type equation on a semi-log plot:

$$F = 1 - \exp(-Br^n) \quad (1)$$

For the metal tested in this work, the constants for 500°C annealing temperature were determined to be 0.0673 and 0.1854 for the coefficient B and exponent, n , respectively. These values are quite low, indicating a slow recrystallization rate as is expected for an aluminum alloy containing a significant amount of Zr [Riddle and Sanders, 2000; Robson and Prangnell, 2001]. As can be seen in Figure 1, the structure was only recrystallized about 40% after annealing at over $0.8 T_m$ (near the melting temperature of some of the constituent particles) for 24 hours. Analysis of various specimens (3-4 analyzed for each condition) yielded results for the recrystallized fraction with a relatively small amount of statistical uncertainty in the measurement. There was less than 20% difference between the maximum and minimum measured values for recrystallized fraction after annealing for one hour.

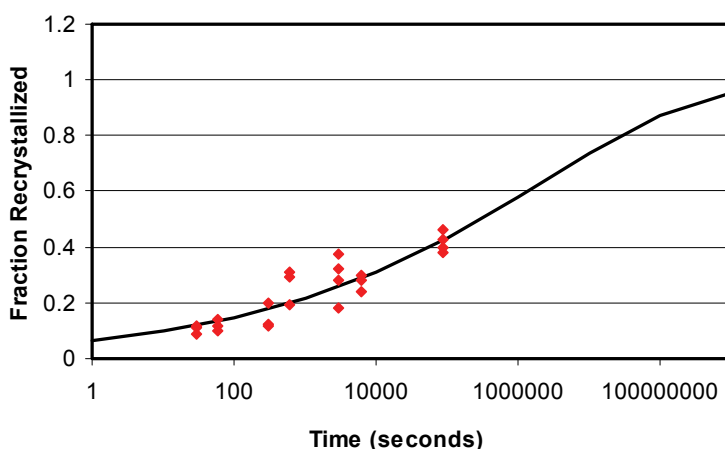


Figure 1: Recrystallization kinetics at 500°C for the AA 7050 material analyzed. Diamond shapes show individual measurements and the solid line is a trend line fit to an Avrami type equation.

It is anticipated that the texture of grains that were recrystallized due to a PSN mechanism will be somewhat randomized, as mentioned above. For determination of the crystallographic texture of recrystallized grains for comparison against the overall texture, EBSD data were identified as being either within a recrystallized grain or in a deformed grain.

3.1 Grain Orientation Spread

Automated identification of recrystallized grains has recently been performed using EBSD data through a measure known as the grain orientation spread (GOS) [Alvi, et al. 2003, Cho, et al. 2006, Field, et al. 2007, Xu, et al. 2009]. GOS is defined

here as the maximum misorientation angle (orientation spread) between any two points considered to be part of a grain. In mathematical form, the GOS can be expressed by:

$$GOS = \frac{1}{N} \sum_{i=1}^N \left\{ \min \left[\cos^{-1} \left(\frac{\text{trace} [g_{ave}(h_i g^A)^{-1}] - 1}{2} \right) \right] \right\} \quad (2)$$

where A indicates the A^{th} measurement position in a grain consisting of N measurements. g_{ave} is the average orientation of the crystallite lattice, and g^A is the measured orientation at the A^{th} position within the grain. h_i is the appropriate symmetry element that yields the minimum misorientation angle between the average orientation and the A^{th} measurement. A grain is defined in EBSD as a contiguous set of measurement positions that are bounded by a misorientation angle that is greater than a given tolerance angle. Historically, a misorientation tolerance angle of 5 to 10 degrees has been used to identify grains, and recrystallized grains are defined by a GOS of 1 or 2 degrees.

An example of GOS being used to track recrystallization in a polycrystalline specimen is shown in Figure 2. Figure 2 contains a series of EBSD images that were obtained at various times from in-situ annealing of a heavily deformed Cu specimen at 155° C [Field, et al. 2007]. Grains are shaded according to GOS with the scale going linearly from white to black corresponding to 0° to 12° in orientation spread. The progress of recrystallization can be tracked by observing the evolution of grains with a low GOS value. The final frame in Figure 2 shows a region of unrecrystallized structure that survives the anneal. This region is readily observed with GOS.

Automated identification of recrystallized grains was attempted using EBSD measurements of the annealed AA 7050 structures. The recrystallized fractions obtained in this manner were compared against those described in Figure 1 (obtained by line intercept counts from optical images). The spread in estimation of the recrystallized fraction at each temperature increased using this method. Closer observation revealed that some of the grains had been mis-identified using the EBSD approach. A simple analysis of the GOS data was performed with an attempt to identify the bi-modal distribution that should exist in a partially recrystallized structure. Figure 3 shows a histogram of these data with the relative intensities of each GOS value plotted for a deformed structure (Fig. 3.a.) and a partially recrystallized structure (Fig. 3.b). While Figure 3.b shows a somewhat bi-modal distribution, as expected, it is apparent that the recrystallized and unrecrystallized regions are not well-separated in this alloy by the GOS measure. The recrystallized grains were therefore identified and flagged for analysis using a point and click method, after

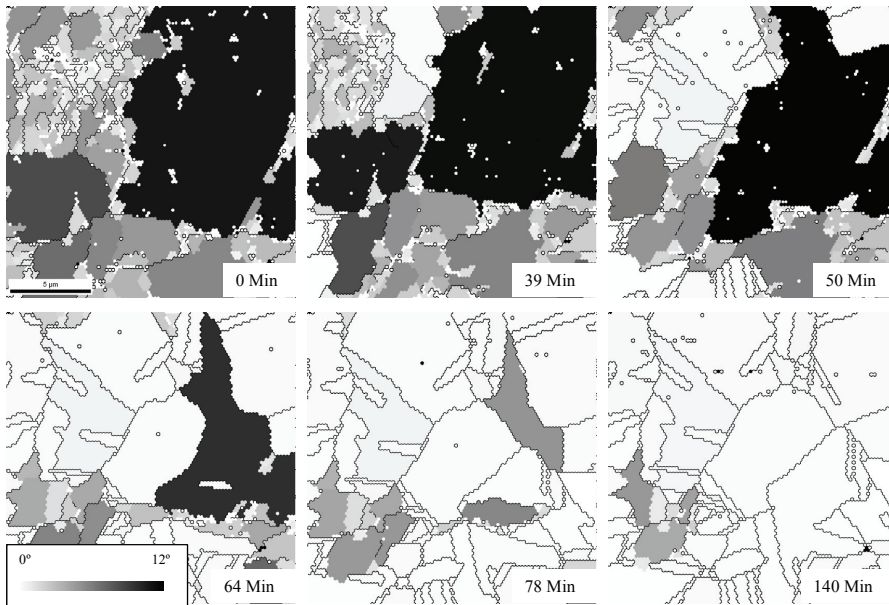


Figure 2: Storyboard presentation of the recrystallization progression being tracked by GOS. The gray regions in the final image (lower right) are regions that are left unrecrystallized at the end of the annealing procedure.

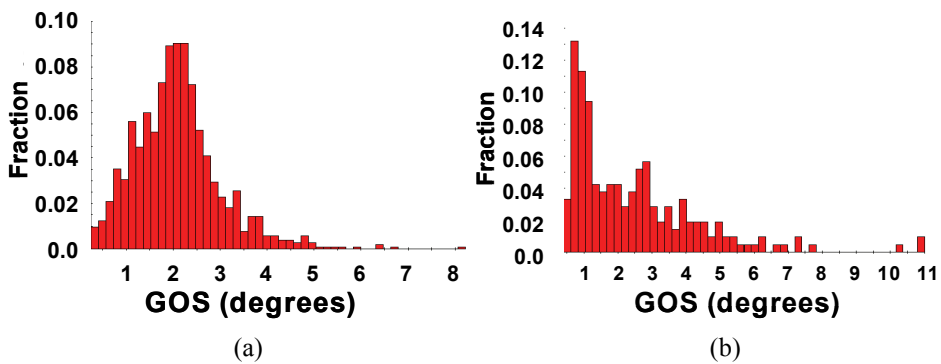


Figure 3: GOS histograms showing representative distributions for (a) unrecrystallized and (b) partially recrystallized structures.

the initial attempt using GOS. This resulted in a similar curve obtained from EBSD data to that shown in Figure 1 (obtained from analysis of optical images).

3.2 *Crystallographic Texture*

From the EBSD data both the orientation and relative positions of the recrystallized grains were obtained. The textures from the deformed structure and from the recrystallized grains for a specimen that had been annealed for 24 hours at 500°C are shown using $\{111\}$ pole figures in Figure 4. The deformation texture is somewhat weak, but the deformed structure shows the expected components of the rolling texture. The orientation distribution of the recrystallized grains appears to be quite random and free from a preferred orientation. The expected texture for a recrystallized plate would consist of various recrystallization texture components, primarily that of the cube texture $\{100\} \langle 001 \rangle$. The observed random orientation distribution is an indication that PSN plays a significant role in the recrystallization process for this alloy.

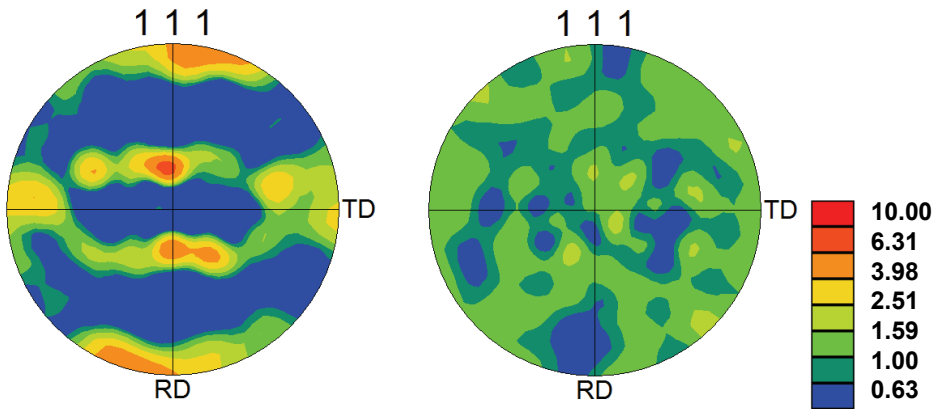


Figure 4: $\{111\}$ pole figures showing textures of (a) the deformed grains and (b) the recrystallized grains from the structure annealed at 500°C for 24 hours. Color scale is in units of “times random” or multiples of random.

3.3 *Pair Correlation Functions*

Another feature of interest is the spatial distribution of the observed particles that may act as nucleation sites for recrystallization. This distribution can be compared with that observed for the recrystallized grains. If these distributions are similar, it provides further evidence that the recrystallization process is dominated by the

PSN mechanism. The distribution of particles that were on the order of 1 micron and larger was observed by means of backscattered electron imaging in the SEM. These particles were predominantly S-phase but a few Fe-rich particles were also observed in the structure. All particles observed are treated identically in this study. Figure 5 shows a representative image with the particles seen as bright spots in the image. The image is taken from the so-called long-transverse section of the plate with the vertical direction of the image aligned with the rolling direction of the plate and the horizontal direction aligned with the normal direction of the plate. Particle positions were reliably identified from these images using gray-scale thresholding with the brighter regions identified as particles. Figure 5.b shows the thresholded image of the same region shown in Fig. 5.a with the particle positions clearly identified. From this image, the centroid of each particle was obtained. Obviously, the size and shape of each particle could also be identified and a complete pair correlation function could be measured. However, the goal of this analysis was to measure the pair correlation function that yields the spatial distribution of the particles and the auto-correlation of the particles is of no interest at this point. We hope only to compare the spatial distribution of particles with that of the recrystallized grains to determine if the distributions are consistent with one another. The pair correlation function for such a two-dimensional distribution can be represented simply as being a function of an angle, θ , and a distance, r . The angle θ is referenced from 0° , aligned with the ND of the plate through 90° , aligned with RD to less than 180° . The correlation function between particles can be determined by comparing only the centroid positions for each particle, in relation to all other particles in the vicinity. The function, $h_{p-p}(r; \theta)$, can be represented mathematically by a Fourier series expansion using appropriate harmonic functions consisting of the Legendre polynomial function and the exponential function in the complex plane,

$$h_{p-p}(r, \theta) = \sum_{l,m} A_{lm} \exp(ilr) P_m(\cos \theta) \quad (3)$$

In this equation, P_m are the Legendre polynomial functions and A_{lm} are the coefficients of the Fourier series expansion.

Figure 6 shows the pair correlation function plotted for the particle distribution. In this case, the reference direction is aligned with the normal direction of the plate, so the 90 degree position is aligned with the rolling direction. It is apparent from the pair correlation that the particles tend to align in the rolling direction (as is obvious from Figure 5). The images used for the measurement of the function were approximately $180 \mu\text{m}$ and $240 \mu\text{m}$ in the rolling and normal directions respectively. This is seen in the function as no correlation exists after $180 \mu\text{m}$ in the rolling direction.

A similar pair correlation function was measured from the distribution of recrystallized grains. The centroid position of each grain was identified and a pair cor-

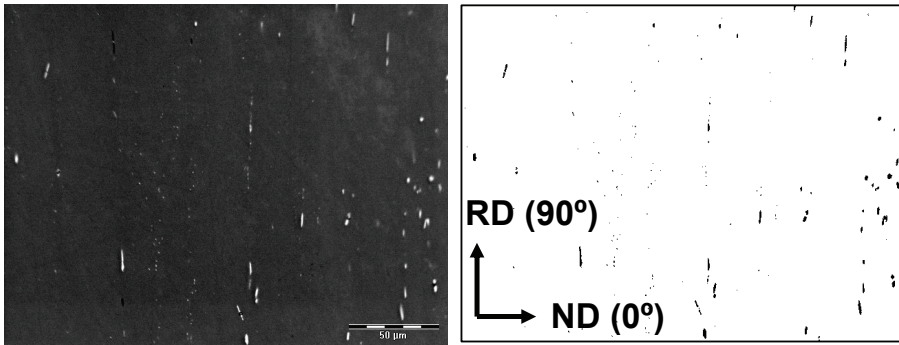


Figure 5: BSE image and thresholded image showing the particle distribution in a representative structure (the micron bar shown is $50 \mu\text{m}$).

relation function was calculated for the overall data. The EBSD maps used in this determination were substantially larger than the images used to measure the particle distribution, therefore, the correlation length was limited to $200 \mu\text{m}$ in the rolling direction and about 250 in the normal direction. Figure 7 shows an orientation image of a structure annealed at 500°C for 5 minutes and the corresponding map of recrystallized grains as defined by GOS. This representative image is similar to the others seen, wherein the recrystallized grains tend to align with the rolling direction in clusters. In Figure 7, gray-scale shaded grains are considered to be recrystallized and white grains are unrecrystallized (according to a GOS definition of 2 degrees. Figure 8 contains the pair correlation function as determined from all such data sets (all data again combined). The pair correlation is similar in nature to that shown for the particle distribution in that the dominant feature is the correlation of grains aligned with the rolling direction.

The details of the distributions vary somewhat as might be expected, but the primary feature is consistent. The scale of the correlation is similar for the particles and the recrystallized grains along the rolling direction (8-16 times random), indicating that this technique gives a second confirmation (along with texture randomization) that nucleation is primarily a result of the PSN mechanism. The quantitative analysis of the particle distribution directly offers an indication of the spatial distribution of recrystallized grains. The extent to which the functions are similar directly indicates the dominance or lack of PSN. The large intensity in the pair correlation for recrystallized grains at longer distances (Fig. 8) that is not seen in the particle distribution is likely a consequence of the sampling technique. The larger images interrogated to measure the pair correlation of recrystallization nuclei allowed a high fraction of measurements at the longer lengths that would not

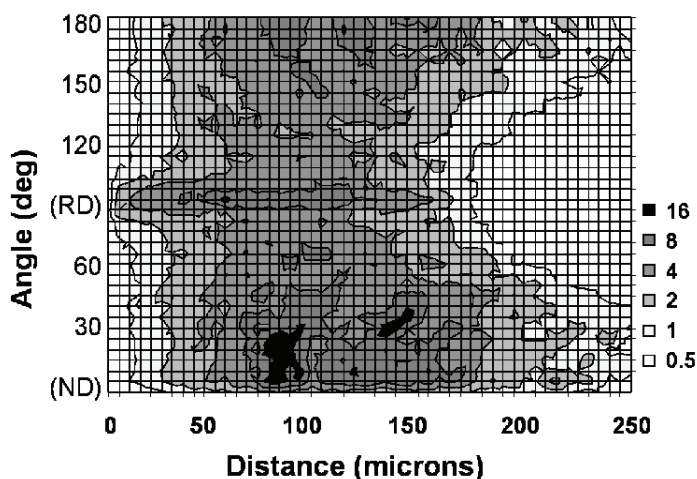


Figure 6: Pair correlation functions showing the relative spatial distribution of particles.

be observed from images on the same scale as those used in measuring the particle distribution.

Finally, all particles seen in the microstructure were counted equally. It is known that the larger particles are more likely to cause a tortuous metal flow, resulting ultimately in PSN. Further work should verify the size of particles that contribute to PSN and that should be included or excluded from the distribution.

4 Conclusions

The alloy of AA 7050 investigated in this study demonstrated recrystallization kinetics that were quite slow. The exponent in the Avrami equation was 0.1854, indicating that recrystallization was impeded by structural constraints. The primary constraint in this structure is assumed to be the Zr rich dispersoids that are known to slow or prevent recrystallization in this alloy. The primary mechanism for nucleation in this alloy was likely that of particle stimulated nucleation. This is evidenced by the weak or random texture of the recrystallized grains. The pair correlation functions for the particle distribution matches that of the recrystallization nuclei along the RD even to the point of quantitative agreement (8-16 times random). This is another indication that recrystallization was dominated by PSN in this investigation and offers a method to quantitatively determine the extent to which PSN contributes to the overall recrystallization of the structure.

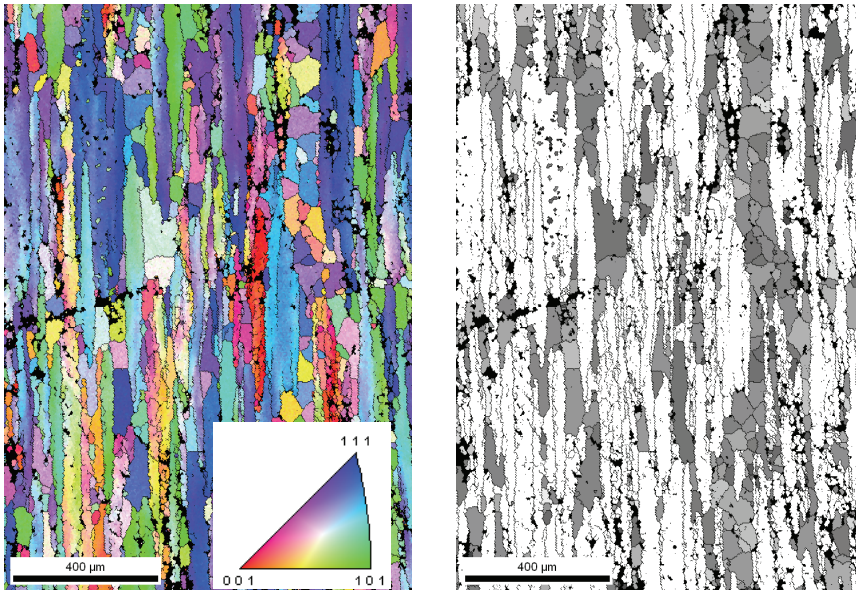


Figure 7: Orientation map and recrystallized grains map for the 7050 alloy annealed 60 minutes at 500°C.

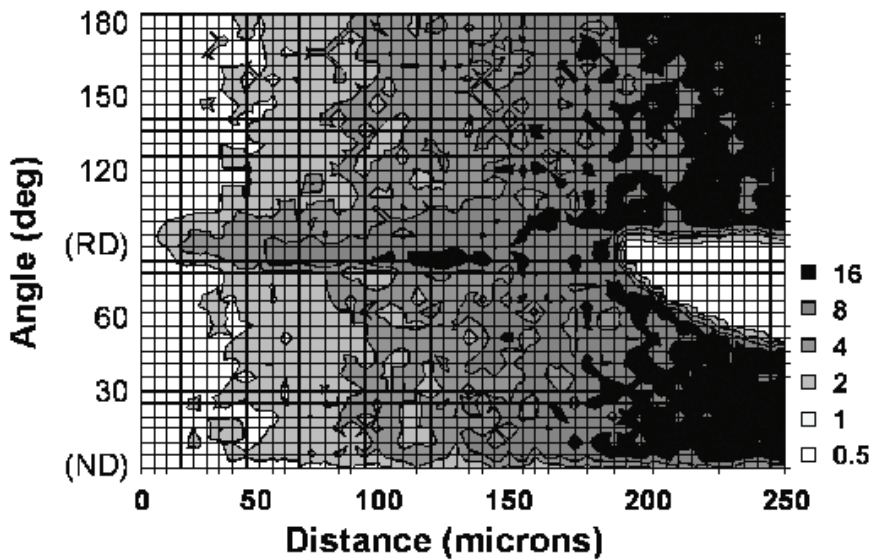


Figure 8: Pair correlation function showing the distribution of recrystallized grains. The gray scale is in units of times random.

Acknowledgement: This work was partially supported by the National Science Foundation's Research Experience for Undergraduates program under grant number DMR-0755055.

References

Adams B.L.; Nylander C.; Aydelotte B.; Ahmadi S.; Landon C.; Stucker B.E.; Ram G.D.J. (2008); Accessing the elastic-plastic properties closure by rotation and lamination. *Acta Mater*, vol. 56, pp. 128-139.

Alvi, A M.H.; Cheong, S.; Weiland H.; Rollett, A.D. (2003); "Microstructural evolution during recrystallization in hot rolled Aluminum Alloy 1050," *Proc. 1st Intl. Symp. on Metallurgical Modeling for Aluminum Alloys*, TMS, Pittsburgh, pp. 191-197.

Ardakani, M.G.; Humphreys F.J. (1994); The annealing behaviour of deformed particle-containing aluminium single crystals. *Acta Metall Mater*, vol. 42, pp. 763-771.

Beaudoin, A.J.; Cassada, W.A. (1998); Investigation of texture and fracture toughness in AA 7050 plate. *Hot Deformation of Aluminum Alloys*, TMS, Pittsburgh, pp. 221-228.

Beran, M.J. (1968); *Statistical Continuum Theories*. John Wiley Interscience, NY.

Beran M.J.; Mason T.A.; Adams B.L.; Olsen T.J. (1996); *J. Mech. Phys. Solids*, vol. 44, pp. 1543-1563.

Chakrabarti, D.J.; Weiland, H.; Cheney, B.A.; Staley, J.T. (1996); Through thickness property variations in 7050 plate. *Matls. Sci. Forum*, vols. 217-222, pp 1085-1090.

Cho, J.H.; Rollett, A.D.; Cho, J.S.; Park, Y.J.; Moon, J.T.; Oh, K.H. (2006); Investigation of Recrystallization and Grain Growth of Copper and Gold Bonding Wires. *Metall Trans*, vol. 37A pp. 3085-3097.

Engler, O.; Kong, X.W.; Yang, P. (1997); Influence of particle-stimulated nucleation on the recrystallization textures in cold deformed Al alloys. Part I – Experimental observations. *Scripta Mater*, vol. 37, pp. 1665-1670.

Field, D.P.; Bradford, L.T.; Nowell, M.N.; Lillo, T.M. (2007); The role of twin boundaries during recrystallization of copper. *Acta Mater*, vol. 55, pp. 4233-4241

Fromm B.S.; Adams B.L.; Ahmadi S.; Knezevic M. (2009); Grain size and orientation distributions: Application to yielding of alpha-titanium. *Acta Mater*, vol. 57, pp. 2339-2348.

Gore, B.E.; Harnish, S.; Padilla, H.; Robinson, B.J.; Beaudoin, A.J.; Dantzig, J.A.; Robertson, I.M.; Weiland, H. (2003); High temperature properties and pro-

cessing of AA 7050. *Hot Deformation of Aluminum Alloys III* TMS, Pittsburgh, PA, pp. 255-262.

Humphreys, F.J. (1977); The nucleation of recrystallization at second-phase particles in deformed aluminium. *Acta Metall*, vol. 25, pp. 1323-1333.

Humphreys, F.J. (1979); Local lattice rotations at second-phase particles in deformed metals. *Acta Metall*, vol. 27, pp. 1801-1812.

Lemmon, T.S.; Homer, E.R.; Fromm, B.S.; Fullwood, D.T.; Jensen, B.D.; Adams, B.L. (2007); Heterogeneous microstructure sensitive design for performance optimization of MEMS switch. *JOM*, vol. 59, pp. 43-48.

McCoy, J.J. (1981); Macroscopic response of continua with random microstructures. In *Mechanics Today, Vol. 6* (ed. S. Nemat-Nassar). Pergamon Press, New York.

Milton G.W. (1981); Bounds on the electromagnetic, elastic, and other properties of 2-component composites. *Phys. Rev. Lett*, vol. 46, pp. 542-545.

Ørsund, R.; Nes E. (1988); Effect of particles on recrystallization textures in aluminium–manganese alloys. *Scripta Metall*, vol. 22, pp. 665-671.

Oscarsson, A. (1991); The effect of nucleation sites for recrystallization on annealing textures and earing in aluminium. *Textures Microstruct.* Vols. 14–18, pp. 447-452.

Riddle, Y.W.; Sanders, T.H. (2000); Recrystallization performance of AA7050 varied with Sc and Zr. Aluminium alloys: Their physical and mechanical properties, Pts. 1-3, *Matls. Sci. Forum*, vols. 331-3, pp. 799-803.

Robson J.D.; Prangnell, P.B. (2001); Dispersoid precipitation and process model in zirconium containing commercial aluminum alloys. *Acta Mater*, vol. 49, pp. 599-613.

Robson, J.D. (2004); Microstructural evolution in aluminium alloy 7050 during processing. *Mat. Sci. Eng. A*, vol. 382, pp. 112-121.

Schafer, C.; Song, J.; Gottstein, G. (2009); Modeling of texture evolution in the deformation zone of second-phase particles, *Acta Mater*, vol. 57, pp. 1026–1034.

Xu, X.; Quadir M.Z.; Ferry M. (2009); A High-Resolution Three-Dimensional Electron Backscatter Diffraction Study of the Nucleation of Recrystallization in Cold-Rolled Extra-Low-Carbon Steel. *Metal. Mater. Trans*, vol. 40A, pp.1547-1556.

